A Computational Approach to Modeling Excitation-Energy Transfer and Quenching in Light-Harvesting Complexes

Chris John,[†,‡] Laura Pedraza-González,[*,†,‡] Elena Betti,[†] Lorenzo Cupellini,[†] and Benedetta Mennucci[*,†]

†*Dipartimento di Chimica e Chimica Industriale, Università di Pisa, via G. Moruzzi 13, 56124 Pisa, Italy*

‡*These authors contributed equally to this work*

E-mail: laura.pedraza@unipi.it; benedetta.mennucci@unipi.it

Abstract

Light-harvesting complexes (LHC) are known to regulate the flux of energy in different light conditions and activate quenching processes to prevent photodamage in case of high light. However, the molecular mechanisms behind these photoprotective processes remain unclear. A widely accepted model suggests an excitation-energy transfer from excited chlorophylls to neighboring carotenoids which finally act as quenchers. Herein, we present a computational protocol to model the energy pathways in the LHC, focusing specifically on the minor CP29 antenna complex of plants. We explore the factors that modulate the switch between light-harvesting and quenched states. The protocol includes modeling the exciton Hamiltonian of the chlorophylls/lutein aggregate, and calculating population dynamics using a kinetic model based on the Redfield-Förster approach. Our analysis reveals a highly tunable excited-state lifetime for the complex, that can switch between quenched and unquenched state depending on the lutein S_1

energy, in accordance with recent experiments. Moreover, we observe that the s-trans lutein conformers are more likely to exhibit the characteristics of the quencher.

1 Introduction

Photosynthesis relies on a complex and delicate machinery that employs light to function but can incur in photodamage if too much light is absorbed by the photosynthetic pigments. In plants and green algae, the light-harvesting complexes (LHCs) that absorb light and funnel the excitation energy towards reaction centers can also regulate this flux in response to variations in light conditions.[1] This regulation is necessary to avoid photodamage to the photosystems themselves, and occurs within LHCs in a mechanism known as non-photochemical quenching (NPQ).[2–8] When NPQ is triggered, chlorophyll (Chl) excitation is readily quenched, providing a fast dissipation channel for the excess energy.

Notwithstanding decades-long work on single LHCs,[9–12] thylakoid membranes,[13] or even intact leaves,[14,15] the mechanisms underlying NPQ remain elusive. Although the ultimate trigger of NPQ is the acidification of the thylakoid membrane, LHCs can switch to quenched conformational states even when isolated.[10,16] Such a conformational switch is thought to affect the pigments, allowing a fast quenching of Chl excitation, reducing its fluorescence lifetime from 2 ns to less than 200 ps.[16]

The exact quenching mechanism of Chl excitation within LHCs is still a matter of debate.[3,14,17] What is more, it is still unclear how such a mechanism can be switched on and off depending on the LHC conformation. The most accepted model for Chl quenching is excitation-energy transfer (EET) to neighboring carotenoids (Cars), which quickly decay to their ground-state, completing the dissipation.[6,9,11,18–21] Such a model explains the reduced excited-state lifetime of the LHCs by comparatively slow EET to the dark S_1 state of the Cars in direct contact with Chls.[19,22] Conformational changes could then modulate the EET coupling between Chls and Cars, explaining the NPQ switch.[18,20,22] However, molecular dy-

namics (MD) simulations have shown that the conformational changes in the LHCs can hardly tune EET couplings by the amount needed to recover the unquenched lifetimes.[23,24]

The difficulties in constructing a model for EET quenching stem from the challenges of accurately characterizing the structural and electronic properties of the quencher. Target analysis applied to transient absorption spectra in different LHCs has revealed that the quencher state does not have the spectral characteristics of S_1, resembling instead the heavily debated S^* state of Cars.[9,11,25,26] This S^* feature was interpreted as a specific conformation of the Cars that is active in quenching.[9,11] In particular, the CP29 minor antenna complex of plants has proven to present this specific behavior.[9]

Recently, by investigating lutein (Lut) embedded in different conformations of CP29[24] through nonadiabatic excited-state dynamics simulations, some of the present authors have shown that different protein conformations differently stabilize the Lut s-trans conformer (in the L1 binding site) with respect to the dominant s-cis one, differing in the first conjugated chain dihedral on the lumenal side.[27] In the same study, it was shown that all the spectroscopic features ascribed to the S^* state are present exclusively in the S_1 state of s-trans conformers: (i) a shorter excited-state lifetime, and (ii) a blue-shifted excited-state absorption (ESA) peak, when compared to the S_1 of s-cis conformer.

Following these findings, in this work, we present a computational protocol aimed at modeling the excited-state lifetime of the LHC and its tuning due to the EET mechanism of quenching. Here, we take advantage of our previous work on CP29[23,24,27,28] and we use the novel protocol to explore a possible connection between the Lut conformation and the switch modulating the light-harvesting and quenching states in CP29.

Our protocol is based on the direct calculation of the energetic factors that drive EET quenching. We compute the S_1 excitation energies and minima for Lut in CP29, and estimate the spectral density for the S_1 state. In addition, we take first-principles estimations of the exciton Hamiltonian of the Chls. Taking advantage of these calculations we improve the previous kinetic models of EET quenching[19,20,22] by employing a Redfield-Förster description

of the exciton dynamics in the CP29 pigment aggregate.

Our calculations predict a substantial spread of excited-state lifetimes depending on the energy of the Lut S_1 state, providing a possible explanation for the switching between quenched and unquenched states. Furthermore, we find that the s-trans Lut conformation is more likely to produce short excited-state lifetimes.

2 The protocol and its validation

The general workflow of the protocol employed in this work to model the EET process in CP29 is presented in Figure 1. Below we describe the theoretical aspects and methodological details of each of the phases of the protocol. We first describe a method to reliably estimate the reorganization energy and spectral density of Lut S_1 in CP29. Then we present the kinetic model used to describe the exciton dynamics and EET quenching.

2.1 Spectral densities of Lut

In order to describe the vibronic lineshape of Lut S_1 absorption, which dictates the spectral overlap with Chl emission, we employ the spectral density formalism. Spectral densities are calculated from normal-mode analysis,[29] which assumes that the potential energy surface of the ground and excited-state is described by the same harmonic potential, but with a shifted equilibrium position. Within this framework, the spectral density of excited-state i can be computed as:

$$J_i(\omega) = \pi \sum_k \omega_k \lambda_{k,i} \delta(\omega - \omega_k) \tag{1}$$

where ω_k and $\lambda_{k,i}$ are respectively the frequency and the reorganization energy for state i along the k^{th} normal mode. The reorganization energy along each normal mode is determined using the expression $\lambda_{k,i} = f_{k,i}^2/2\omega_k^2$, where $f_{k,i}$ is the excited-state gradient at the Franck-

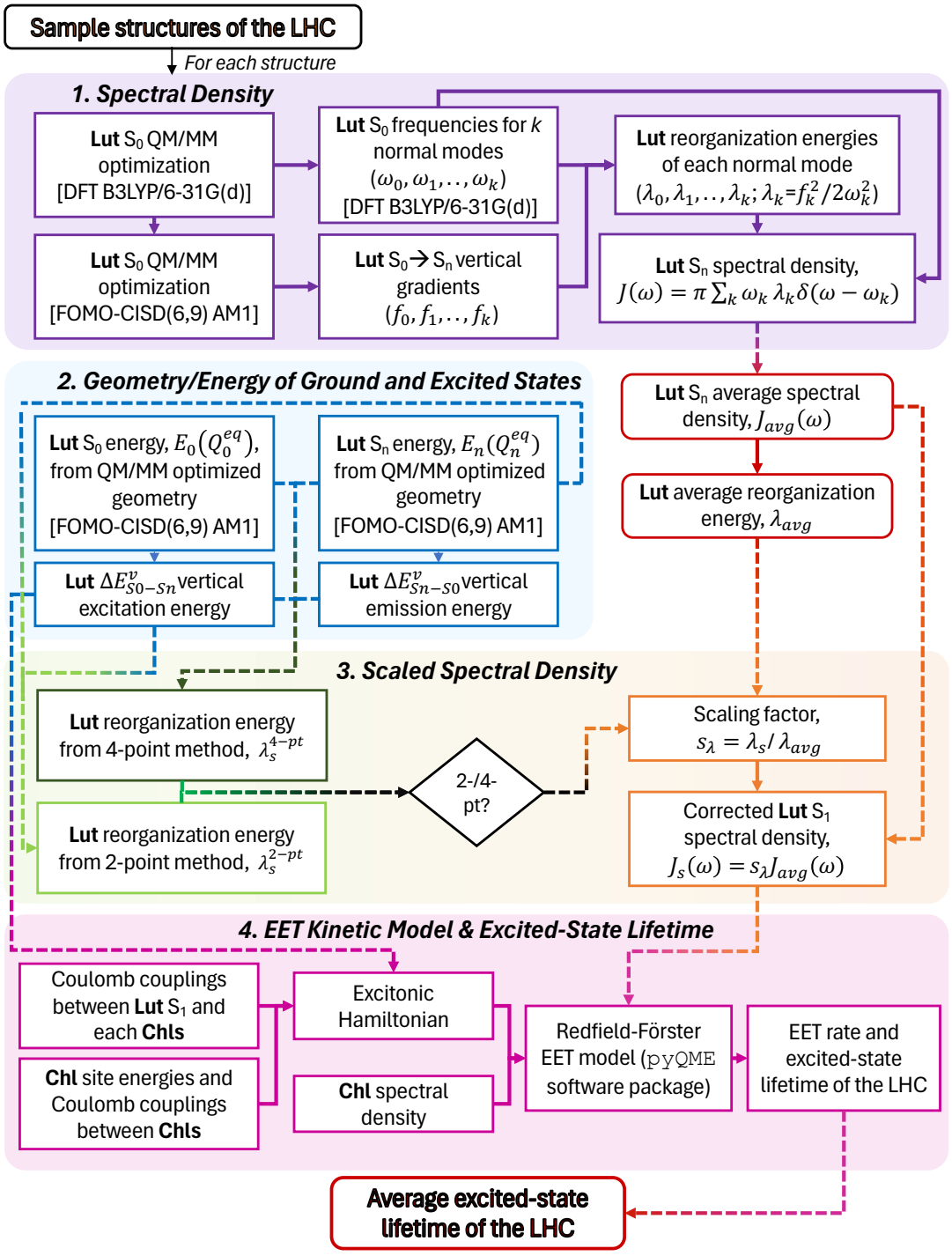

Figure 1: General workflow of the computational protocol to calculate the excited-state lifetime of the LHC. The protocol involves four major steps: (1) calculation of an average spectral density for Lut S_1, (2) evaluation of ground-state and excited-state energies and gradients, (3) rescaling of the spectral density and (4) implementation of the EET kinetic model.

Condon point (vertical gradient).[29,30] The total reorganization energy in this model is

$$\lambda_i = \int_0^\infty \frac{J(\omega)}{\pi\omega} \mathrm{d}\omega = \sum_k \lambda_{i,k} \tag{2}$$

and corresponds to the energetic shift between the vertical excitation energy and the energy of the excited-state minimum.

Since the individual Lut intramolecular vibrational frequencies and normal modes that describe the harmonic motion are about a local minimum reference geometry, a reasonable sampling of the protein conformations is necessary in order to account for the fluctuations on the ground-state potential.[29,30] Our group recently reported a conformational landscape of CP29, explored through enhanced sampling molecular dynamics simulations (in protein membrane)[24] starting from the Cryo-EM structure from spinach (PDB: 3JCU[31]). Herein, we have selected 113 structures of CP29 from this conformational landscape that are well representative of the Cryo-EM geometry as well as the extremes of the landscape. All the sampled structures were refined using a three layer QM/MM optimization:[24] a mobile QM part composed solely of Lut treated at the DFT B3LYP/6-31G(d) level of theory, a mobile MM part composed of residues within 6 Å of Lut, and a fixed MM part that includes the rest of the system (*i.e.*, pigments, lipids, waters, and protein). The protein and lipids were described using AMBER ff14SB[32] and lipid14[33] force fields, respectively, water molecules using TIP3P,[34] while *ad-hoc* parameters were used for the pigments.[35,36] The QM/MM frequency calculations were also performed using the same method, but keeping the whole MM part frozen. These calculations were carried out with the Gaussian 16[37] software.

To describe the first two excited-states of Lut we used multireference semiempirical QM/MM calculations, with Lut as the QM part and the environment (*i.e.*, all residues within 30 Å of Lut) treated as a fixed MM part described using the force field parameters detailed above. More specifically, we employed the AM1 Hamiltonian explicitly reparametrized for Lut on DFT and experimental data.[38] The method has recently shown to properly describe

the electronic structure of carotenoids, including Lut.[24,27,38–41] We used the floating occupation molecular orbital (FOMO) framework,[42] with a Gaussian width for floating occupation of 0.1 Hartree, and we considered all the single and double excitations (CISD) in an active space of six electrons in nine molecular orbitals. We computed the excited-state vertical gradients along the normal modes in the minimum geometry S_0 obtained within the same semiempirical level of theory. All the semiempirical QM/MM calculations were performed using a development version of the MOPAC code,[43] interfaced with the TINKER 6.3 package.[44]

Finally, we combined the obtained data of frequencies and vertical gradients to compute the Lut S_1 and S_2 spectral densities for each of the selected structures using eq. (1). The average spectral densities thus obtained are compared in Figure 2a. Both spectral densities present a similar shape, with three main peaks at about 1580, 1200, and 1040 cm^{-1}, corresponding to the observed Raman-active modes of Lut.[45] This indicates that the normal modes coupled to the excitation are correctly identified by our calculation. Interestingly, the S_1 spectral density shows the same peaks but with a much larger intensity, meaning that S_1 is more strongly coupled to the same modes.

2.2 Validation of the spectral density

To validate the calculated spectral densities we computed the absorption spectra of Lut in CP29. As experimental absorption spectra are available only for the bright S_2 state,[46] a direct comparison is reported in Figure 2b for this state. All spectra shown in this article have been computed with the Python3-based pyQME software package,[28,47] developed in our group.

The calculations predict an absorption band much narrower than the experiment, and with a less pronounced vibronic progression. This discrepancy arises from the approximate nature of the vertical gradient approach[48] and from the use of two different methods in the ground-state frequency and excited-state gradient calculation (see Figure 1). To address and

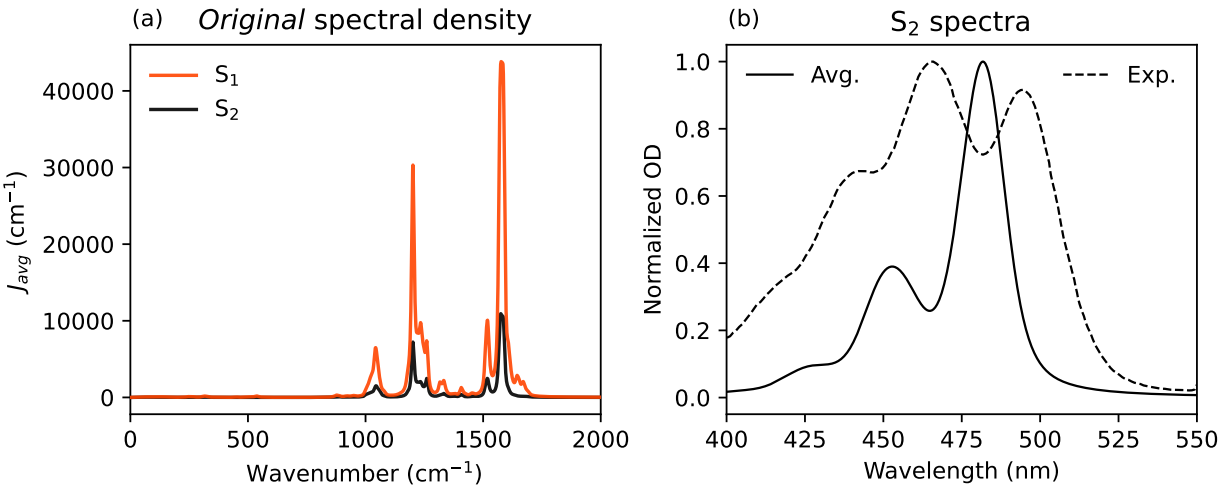

Figure 2: (a) Spectral density computed for the dark S_1 state (orange) and the bright S_2 state (black) of Lut in the CP29 complex. Data is plotted as the average value obtained by using the protocol outlined in Figure 1. (b) The average S_2 spectrum of Lut in CP29 computed using the protocol outlined in Figure 1 for structures sampled from the molecular dynamics reported in Ref. 24, along with the experimental spectrum of Lut S_2 taken from Ref. 46.

overcome these limitations, and account for the full potential energy change in the excited-state between the ground- and excited-state minimum, we use an independent method to compute the total reorganization energy λ. We then scale the spectral density so that the reorganization energy calculated by eq. (2) matches the calculated λ. This scaling is justified by the fact that the normal mode analysis could identify the frequencies coupled to the excitation, although the total reorganization energy was underestimated.

We employed two different strategy to compute the reorganization energy. We firstly employed the 2-point method, namely adiabatic potential method[49] (see Figure 3a). This is the most direct approach to calculate the reorganization energy of an excitation process, namely:

$$\lambda_s^{2-pt} = \lambda_f = E_1(Q_0^{eq}) - E_1(Q_1^{eq}) \tag{3}$$

where Q_0^{eq} and Q_1^{eq} are the optimized geometries of S_0 and S_1 states. The reorganization energy thus defined can also be interpreted as the reorganization energy of the forward reaction (λ_f).

Alternatively, we tested the 4-point method (see Figure 3b) which is commonly employed for electron transfer reactions.[50] The 4-point method defines reorganization energy using the diabatic representation of the potential energy surfaces and assumes a Gaussian distribution for the diabatic states. Following these assumptions, the reorganization energy can be written as

$$\lambda_s^{4-pt} = (\lambda_f + \lambda_b)/2 = (\Delta E^v_{S0-S1} - \Delta E^v_{S1-S0})/2 \tag{4}$$

where λ_b is the reorganization energy of the backward reaction computed as $E_0(Q_1^{eq}) - E_0(Q_0^{eq})$ and, ΔE^v_{S0-S1} and ΔE^v_{S1-S0} are the vertical excitation ($S_0 \rightarrow S_1$) and emission ($S_1 \rightarrow S_0$) energies, respectively (see Figure 3b).

The 2- and 4-point reorganization energies have been calculated for each structure of the LHC, optimizing the geometries of S_1 and S_2 states of Lut with the same QM/MM approach used for vertical gradients (see above). The obtained reorganization energies were finally used to rescale the *original* spectral densities.

To evaluate the performance of the 2-point and 4-point methods in correcting the *original* spectral density, we recalculated the average S_2 spectrum of Lut using the corresponding scaled spectral densities. λ_s^{2-pt} and λ_s^{4-pt} are on average ≈ 2.1 and ≈ 2.6 times greater than the *original* reorganization energy, respectively, confirming that the initial procedure leads to an underestimated value. Remarkably, as seen in Figure 3, a significant improvement is obtained with respect to the spectrum from the *original* spectral density (Figure 2b). Both methods give reasonable agreement with the experiment, with the spectrum from 2-point being slightly better.

2.3 Kinetic model and excited-state lifetime of the complex

The kinetic model we present here is an extension of the one introduced in a recent work by some of us,[28] where a combined Redfield-Förster approach, implemented in the pyQME software package,[28,47] was used to describe the EET processes within a Chl aggregate. Herein

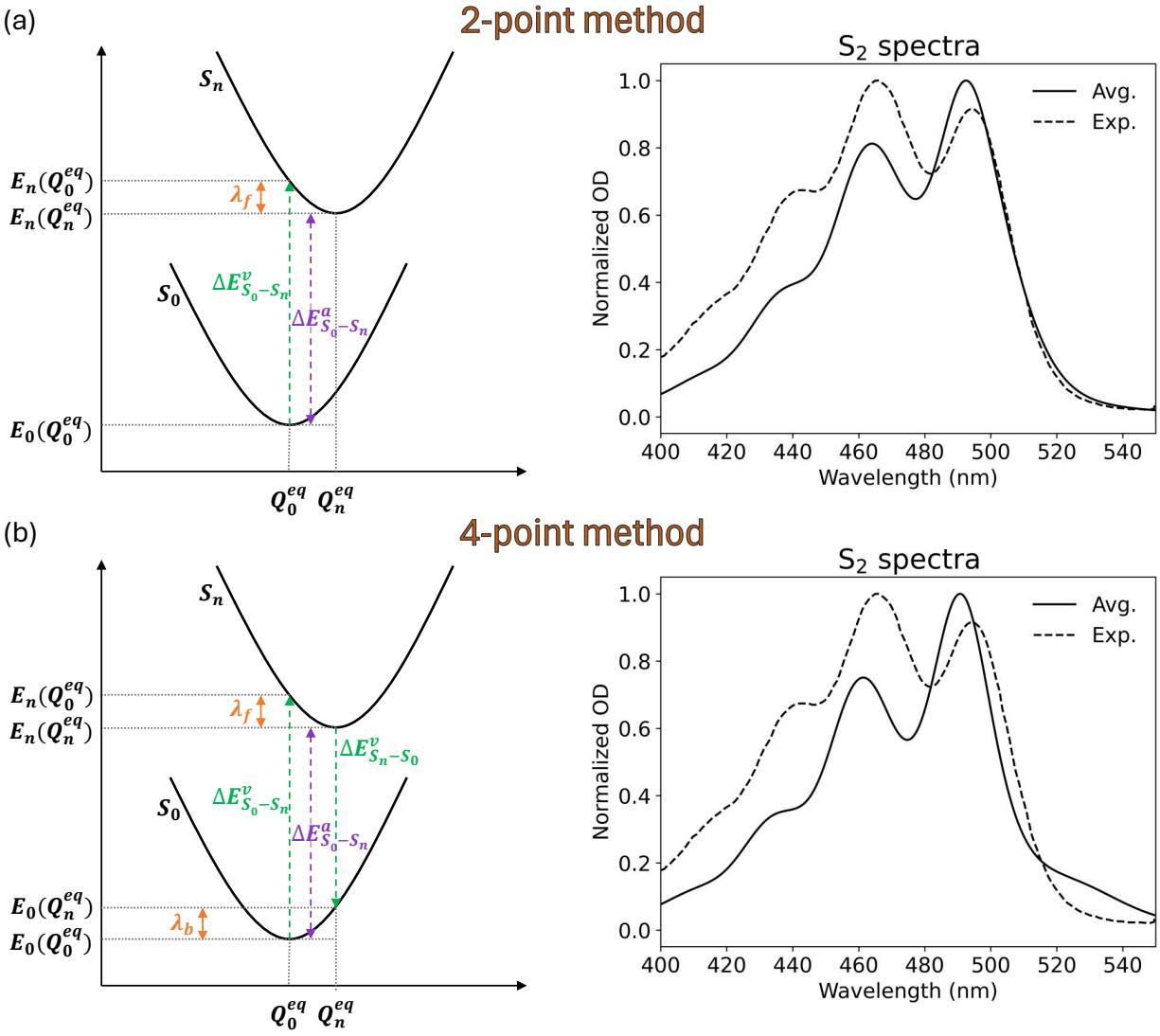

Figure 3: (left panel) Schematic representation of how scaled reorganization energy is obtained from (a) 2-point and (b) 4-point methods. (right panel) Lut S_2 spectra in CP29 computed from the spectral density scaled with (a) 2-point and (b) 4-point methods.

we add the Lut S_1 state to this model in order to simulate the EET quenching. In the following, we briefly summarize the fundamental ingredients of the model; more details can be found in Section S1 and in Ref. 28.

2.3.1 Exciton Hamiltonian

First, the model needs as input the exciton Hamiltonian of the pigments' aggregate, defined as:

$$\hat{\mathcal{H}}_{\text{exc}} = \sum_{i}^{n} \mathcal{E}_i |i\rangle\langle i| + \sum_{i \neq j}^{n} V_{ij} |i\rangle\langle j| \tag{5}$$

where $\mathcal{E}_i$ denotes the vertical transition energy, or site energy, of pigment i and V_{ij} is the coupling between excitations of pigments i and j.

The Lut site energies ($\mathcal{E}_i = \Delta E^v_{S0-S1}$) were computed using the same semiempirical QM/MM method used for the reorganization energies (see Figure 1). In this case we used 271 structures of CP29 sampled along a set of ground-state QM/MM thermal equilibrations (at 300 K) recently reported by some of us.[38] For each structure, the geometry of Lut was refined through a constrained QM/MM optimization in which all the Lut dihedral angles (*i.e.*, around single and double bonds) were kept frozen. With this optimization, we remove all the effects of fluctuations in bonds and angles already treated in the spectral density formalism. To validate this ensemble, we compared our $S_1 \rightarrow S_n$ ESA spectra (see Figure S1) with those calculated in Ref. 27 on a much larger set of structures. Remarkably, the spectra computed from our sample of 271 structures mirror the contributions from the different S_n states (S_5-S_9) reported in Ref. 27, confirming that the structures are representative of the ensemble. An average value of the Lut site energies computed for the sampled geometries is provided in Table 1.

The site energies of the 12 Chls of CP29 and all the Chl-Chl couplings were taken from Ref. 28. Those calculations were repeated over more than 600 MD frames to sample disorder induced by thermal fluctuation of the protein; here a subset of 127 geometries and relative set of sites and couplings is considered.

To account for the different quantum chemical method employed for Chls and Lut, we applied the constant shift determined in Ref. 28 to the Chl site energies.

Data for Lut are combined with the ones for Chls in the following way: for each Lut structure, we compute the S_1 site energy and add it to the Hamiltonian of each different realization of disorder sampled for the Chls, so that 127 Hamiltonians are finally obtained for every Lut structure. Since Chl-Lut(S_1) couplings are known to show only minor variations and have a small effect on modulating the transfer efficiency,[23,24] for each Hamiltonian, we included the same Chl-Lut couplings as taken from Ref. 23. The procedure was then repeated over all the 271 structures. This enables a good description of Lut structural variability while still accounting for relative fluctuations of the Chls-Lut energy gaps.

2.3.2 Rates and population dynamics

The quantum dynamics is simulated using the Redfield-Förster approach. Accordingly, the exciton Hamiltonian matrix is partitioned in blocks, representing pools of strongly coupled pigments. Couplings within the same block produce delocalization of excited-states, while couplings outside of the blocks act as perturbations that promote energy transfer between electronic states of distinct blocks. In this work, according to previous results,[28] the pigments are partitioned as: a601, a602-a603-a609, a604, b606-b607, b608, a610-a611-a612, a613 and separate compartments for Lut(S_1) and global ground-state (GS) (Figure 4a). The diagonalization of the partitioned exciton Hamiltonian yields the exciton states, which are qualitatively depicted on the top left of Figure 4c, with the same color code shown in Figure 4a for the clusters and introduced in Ref. 28. As a consequence of partitioning, exciton states only involve pigments of the same compartment; so by construction no delocalization occurs between the Chls and the Lut. In the majority of the realizations of disorder, the exciton with Lut S_1 character is the highest one, as a consequence of its higher vertical energy compared to the Chls. However, unlike the Chls, the Lut vertical excitation energy is extremely sensitive to the sampled geometry, and this variability in energy is represented

in Figure 4c.

The exciton states are used as a basis for the excited-state dynamics. The evolution of the density matrix is computed by solving a quantum master equation in a secular-Markov approximation. Relaxation among excitons belonging to the same compartment is treated according to the Redfield equation, which describes coherent transfers among delocalized states. Transfers among excitons of different compartments are instead described by Generalized Förster (GF) rates, which model transfers as incoherent hops in a delocalized picture (exciton states are used as a basis instead of pigment states as in standard Förster formulations).[30,51] The EET rate between excitons a and b pertaining to different compartments can be calculated as:

$$K_{b\to a} = \frac{1}{2\pi\hbar^2}\left|\sum_{ij} c_{ia}c_{jb}V_{ij}\right|^2 \times \int_{-\infty}^{\infty} \Phi_b(\omega)A_a(\omega)\mathrm{d}\omega \tag{6}$$

where c_{ia} are the exciton coefficients, $A_a(\omega)$ is the absorption lineshape of exciton a and $\Phi_b(\omega)$ is the fluorescence lineshape of exciton b. The integral therefore corresponds to the spectral overlap between the emission of the exciton state b and the absorption of exciton state a. Details are provided in Section S1.

The spectral densities are fundamental input quantities of the EET kinetic model: they appear explicitly in the expression of the Redfield rates (see Section S1) and are also needed to compute both the spectral lineshapes appearing in eq. (6). In our model, the spectral density for the Chls are taken from Ref. 52, while for Lut we use the S_1 scaled spectral density (*i.e.*, 2-point or 4-point) computed for each sampled CP29 structure. The extent of the spectral overlap, between the Lut absorption spectrum ($S_0 \to S_1$) and the Chl aggregate fluorescence, obtained with these data is illustrated in Figure 4b.

Empirical rates to the GS are added to the Redfield-Förster rate tensor and set to a fixed value, according to experimental evidence of typical lifetimes: 4 ns for excitons involving Chls[9] and 14 ps to the exciton localized on Lut.[20,53] A scheme illustrating our EET

kinetic model is shown in Figure 4c. In the figure we show that EET occurs towards the S_1 minimum of Lut. Within the generalized Förster rate, detailed balance is ensured between the minima of the excited-states. In other words, the adiabatic excitation energies, $\Delta E^a_{S0-S1} = \Delta E^v_{S0-S1} - \lambda$, dictate the equilibrium between forward and backwards rates.

The population dynamics is recomputed for each Hamiltonian detailed above, then transformed to the site basis and finally averaged over the disorder. We used an initial condition localized on the a610-a611-a612 domain. Other choices gave negligibly different results in the overall quenching dynamics, as the latter is much slower than the equilibration time between Chls.

3 The excited-state dynamics

In this section, we first evaluate the model depicted in Figure 1 in a set of diverse CP29 structures and report the average excited-state lifetime. In doing so, we employed the two approaches introduced above for the estimation of Lut S_1 reorganization energy and compared the obtained EET kinetic models. Secondly, we assess how varying the Lut S_1 energy modulates the excited-state lifetime and, in turn, the extent of quenching in CP29. Finally, in Section 3.2 we use the same data to investigate whether a change in Lut conformation (*i.e.*, from s-cis to s-trans) may represent a switch between a quenched and a light-harvesting state.

3.1 All pigment Chl–Lut(S_1) EET model

By using the Redfield-Förster model presented in Section 2.3, we computed the evolution of excited-state population upon Chl excitation in the CP29 complex. As can be seen in Figure 5, we report the average populations obtained with both 2-point (Figure 5a) and 4-point (Figure 5b) schemes. The solid lines represent the population evolution of the different pigment pools and the GS. In the timescales shown in Figure 5, all Chl pools decay with the

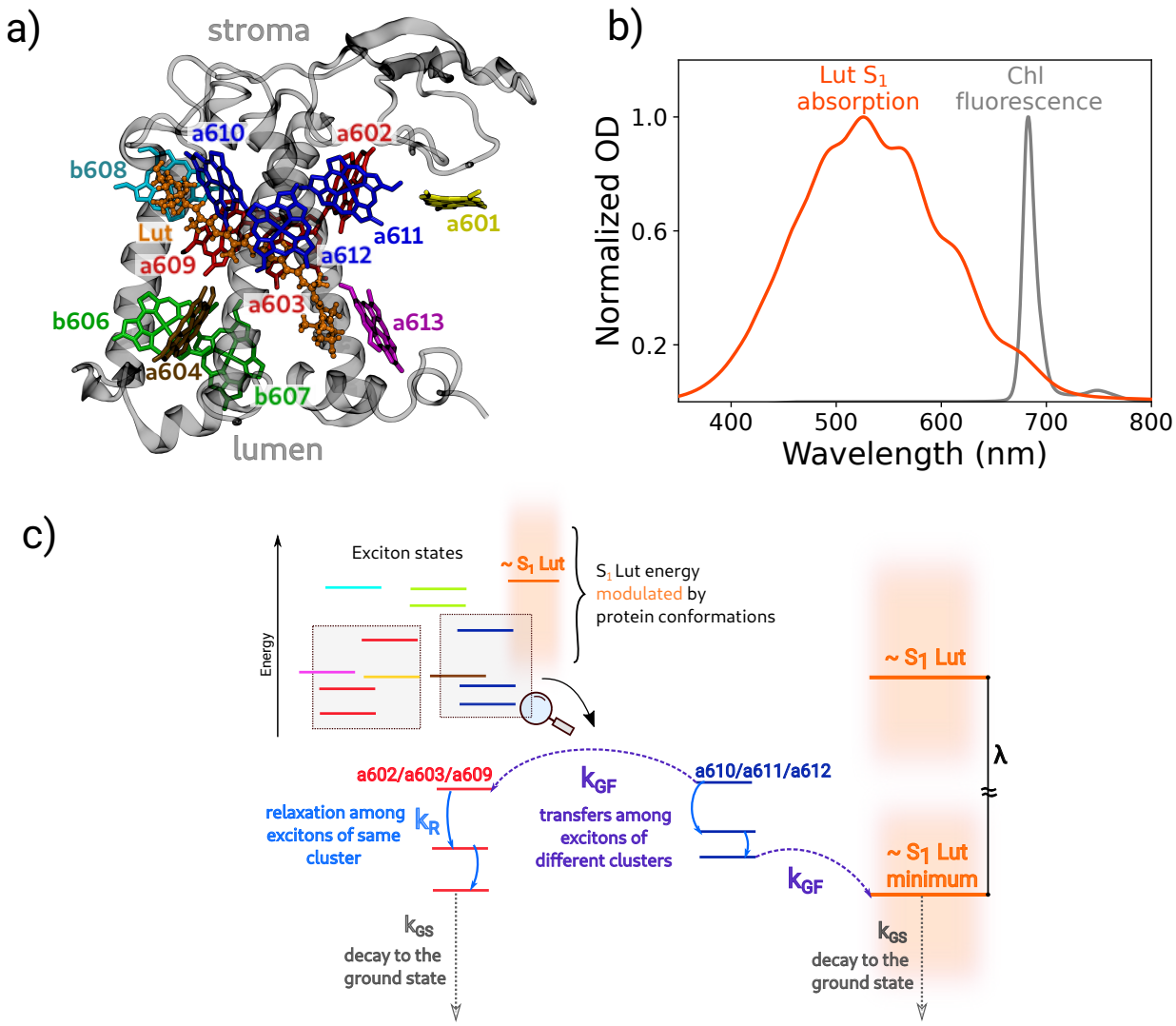

Figure 4: All pigment EET model for CP29. Panel (a): structure of CP29 protein showing the 12-pigments Chl aggregate and the Lut in site L1. The color code for Chls is the same of Ref. 28 and shows the partition in strongly coupled pools, while Lut is presented in orange. (b) The spectral overlap between Lut S_1 absorption and Chl fluorescence. (c) Qualitative depiction of the exciton states (top left) and of the kinetic model used to describe the population dynamics. With $\sim S_1$ we refer to the exciton localized on Lut; its variability among the Lut structures is shown by the rectangles shaded in orange. The minimum of S_1 is also shown for comparison with Chls exciton energies (see Section 3.1 for comments).

same rate, because the equilibration among Chls is much faster than the decay to the GS. The population of Lut S_1 remains always low, as this state decays faster than it is populated. This kind of inverted kinetics has to be taken into account in the target analysis of transient absorption spectra.[9]

To compare our model with time-resolved fluorescence experiments,[9] we present (dashed line in Figure 5a,b) the total excited-state (ES) population of the complex, which is obtained by summing the contributions from each pigment. The excited-state lifetime of the entire complex can be determined by fitting the excited-state population. While the average kinetics is in principle multiexponential, the GS recovery can be approximated using a single exponential with lifetimes of $\tau = 284$ ps and 1232 ps for Figure 5a and 5b, respectively.

To gain further insight into the modulation of the quenching rate, we plotted the excited-state lifetime τ for each of the of the 271 structures (see Section 2.3) in Figure 5c,d, and compared it to the adiabatic Lut S_1 excitation energy calculated for the same structure. As expected, τ correlates well with the S_1 energy, as lower energies entail a larger spectral overlap with the Chl exciton emission (see Figure 4b), leading to a higher EET rate. The behavior of this correlation varies depending on the model used to estimate the reorganization energy. With the 2-point method, there is a nearly perfect correlation between lifetime and adiabatic S_1 energy, because the effective adiabatic excitation energy that enters the generalized Förster rate matches the one calculated from the S_1 and S_0 minima, *i.e.*, $\Delta E^a_{S0-S1} = \Delta E^v_{S0-S1} - \lambda_s^{2-pt}$, as shown in Figure 3a and Table 1. However, with the 4-point method, the relation is more approximate because the reorganization energy is computed differently (Figure 3b), leading to a discrepancy between ΔE^a_{S0-S1} and $\Delta E^v_{S0-S1} - \lambda_s^{4-pt}$, as shown in Table 1.

Importantly, for both sets of reorganization energies, our calculations predict a wide range of excited-state lifetimes, from ca. 70 ps to over 2 ns. Moreover, significant variations in τ occur with a small change in energy (~ 0.15 eV). This sensitivity can be explained by noting that the Chl exciton energy lies at the very red edge of the S_1 absorption lineshape (see Figure 4b). As a consequence, even small changes in the S_1 energy can substantially

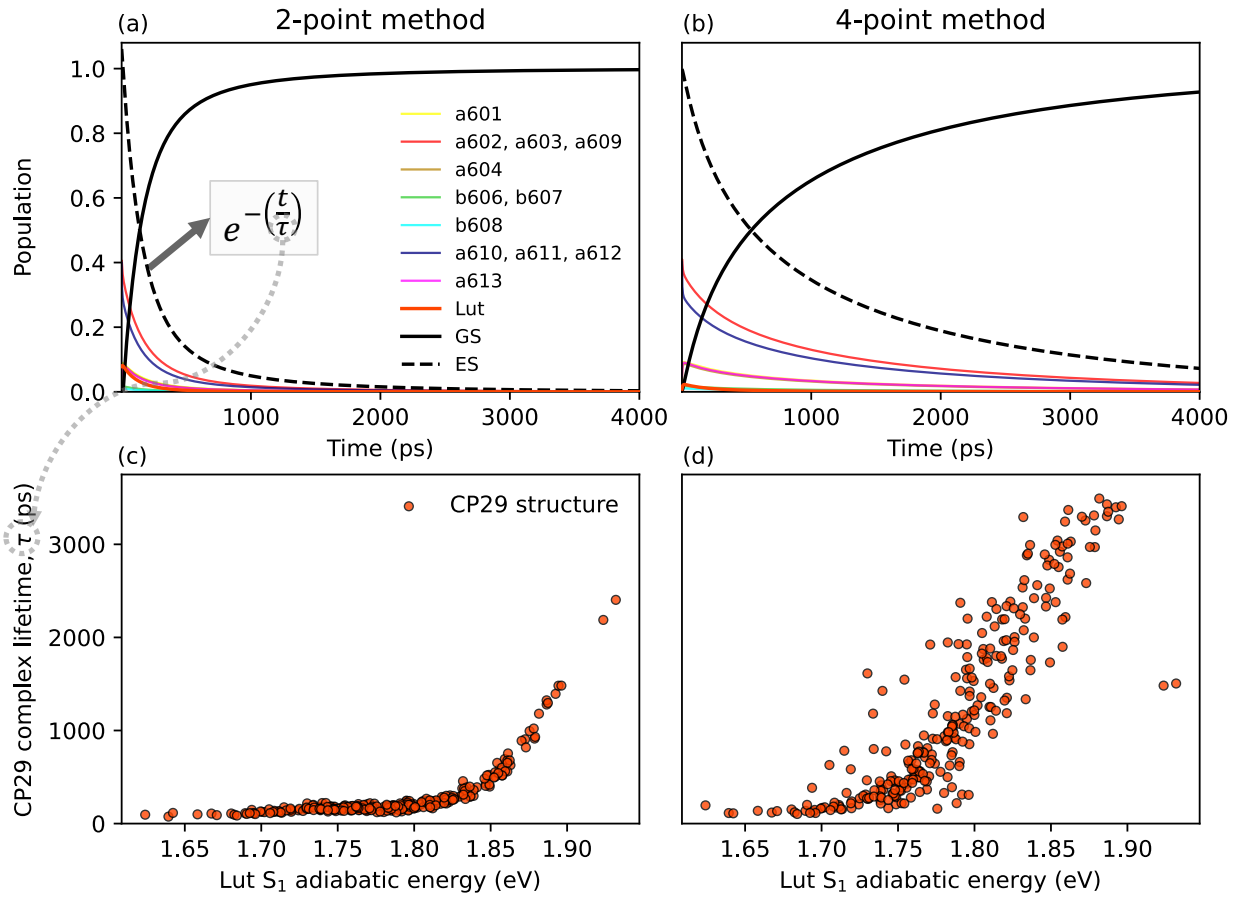

Figure 5: (top panel) Population evolution of the different pigment pools and the global ground (GS) and excited-state (ES) of the entire system evaluated using the EET model represented in Figure 4. The Lut spectral density used in the EET model is scaled using the (a) 2-point and (b) 4-point methods. (bottom panel) Modulation of the excited-state lifetimes by S_1 adiabatic energies for (c) 2-point and (d) 4-point methods.

affect the Chl → S_1 EET rate. The large sensitivity to the Lut S_1 energy also accounts for the difference in lifetimes obtained with the two sets of reorganization energies. Since our calculations revealed a better correlation between the lifetime and Lut S_1 energy in the case of the 2-point method than the 4-point, from here on we will employ the 2-point method.

Table 1: The average values and standard deviations of vertical (ΔE^{v}_{S0-S1}) and adiabatic (ΔE^{a}_{S0-S1}) excitation energies of Lut S_1 and, the reorganization energies (λ_s) computed with the 2-point approach and the corresponding values for 4-point approach.

	Lutein S_1		2-point		4-point	
Structures	$\langle \Delta E^{v}_{S0-S1} \rangle$ (cm^{-1})	$\langle \Delta E^{a}_{S0-S1} \rangle$ (cm^{-1})	$\langle \lambda_s \rangle^{\dagger}$ (cm^{-1})	$\langle \Delta E^{v}_{S0-S1} - \lambda_s \rangle$ (cm^{-1})	$\langle \lambda_s \rangle^{\dagger}$ (cm^{-1})	$\langle \Delta E^{v}_{S0-S1} - \lambda_s \rangle$ (cm^{-1})
all	18978 ± 493	14506 ± 437	4471 ± 286	14506 ± 437	3643 ± 206	15334 ± 356
s-cis	19182 ± 485	14646 ± 436	4535 ± 210	14646 ± 436	3729 ± 174	15452 ± 350
s-trans	18879 ± 469	14520 ± 377	4359 ± 253	14520 ± 377	3554 ± 192	15325 ± 316

† See Figure 3 for a schematic representation of 2-point and 4-point methods.

3.2 Effect of Lut conformation on excited-state lifetime

We now investigate whether the Lut conformation influences the excited-state lifetime and, in turn, the extent of quenching in CP29. To this aim, we divided our sample structures into two groups corresponding to the Lut s-cis and s-trans conformation, respectively (Figure 6a).

As a first step of the analysis, we plotted the average population evolution of the s-cis and s-trans structures separately, to closely examine how the kinetics of the various pigments are influenced by the Lut conformation. These results are presented in Figures 6b,c. We observed a quantifiable difference between the average population evolution of the s-cis and s-trans conformers, with the GS being populated more quickly in the case of s-trans than s-cis. This is a consequence of a larger overlap of the s-trans S_1 state with the Chl excitons which subsequently results in a more populated S_1 state and a faster decay to the GS. For further analysis, we artificially applied a blue shift of 500 cm^{-1} to the excitation energies of

both s-trans and s-cis Lut, which led to fewer structures with an effective spectral overlap with Chl emission. For both s-cis and s-trans conformers, this resulted in a slower average decay to the GS. At the same time, we observed a larger difference in the excited-state decay of the s-cis and s-trans conformers.

Transient absorption experiments upon excitation of the Chls in CP29 have suggested that the quencher state corresponds to a specific conformation of Lut with blue-shifted excited-state absorption.[9,25] To connect our results with these experiments, we analyzed the lifetime of each structure from the s-cis and s-trans groups. As illustrated in Figure 7a, there is a slightly larger proportion of geometries with the s-cis conformation in the nanosecond lifetimes region. Instead, if we look at the "quenched" structures with lifetimes of the order of ∼100 ps, we find a larger proportion of s-trans geometries. Greater population of Lut S_1 is also more likely for the s-trans conformer (Figure 7b). In transient absorption experiments, the signal of the quencher state (*i.e.*, Lut S_1) is proportional to its population. For this reason, we expect that the S_1 signal measured in these experiments would more likely arise from s-trans.

It is important to note that our calculations do not predict a hard switch between Lut conformations. In fact, both conformations present a rather continuous distribution of lifetimes (Figure 7c), instead of a clear separation. Target analysis of transient absorption spectra can disentangle contributions from different conformations,[9] but requires some assumptions, and usually cannot distinguish many different timescales. Therefore, our picture is not in disagreement with the experiments on CP29. Nonetheless, within our results the Lut conformation alone is not sufficient to explain the difference in lifetimes observed[9] between strongly quenched (∼60 ps) and unquenched (∼3 ns) CP29.

We can put forward different reasons for this finding. First, the modulation of the S_1 energy of Lut likely results from a combined effect of its internal conformation and protein-induced distortions. Consequently, the conformation of Lut alone may not fully explain the modulation, and a more detailed investigation of the protein environment is necessary to fully

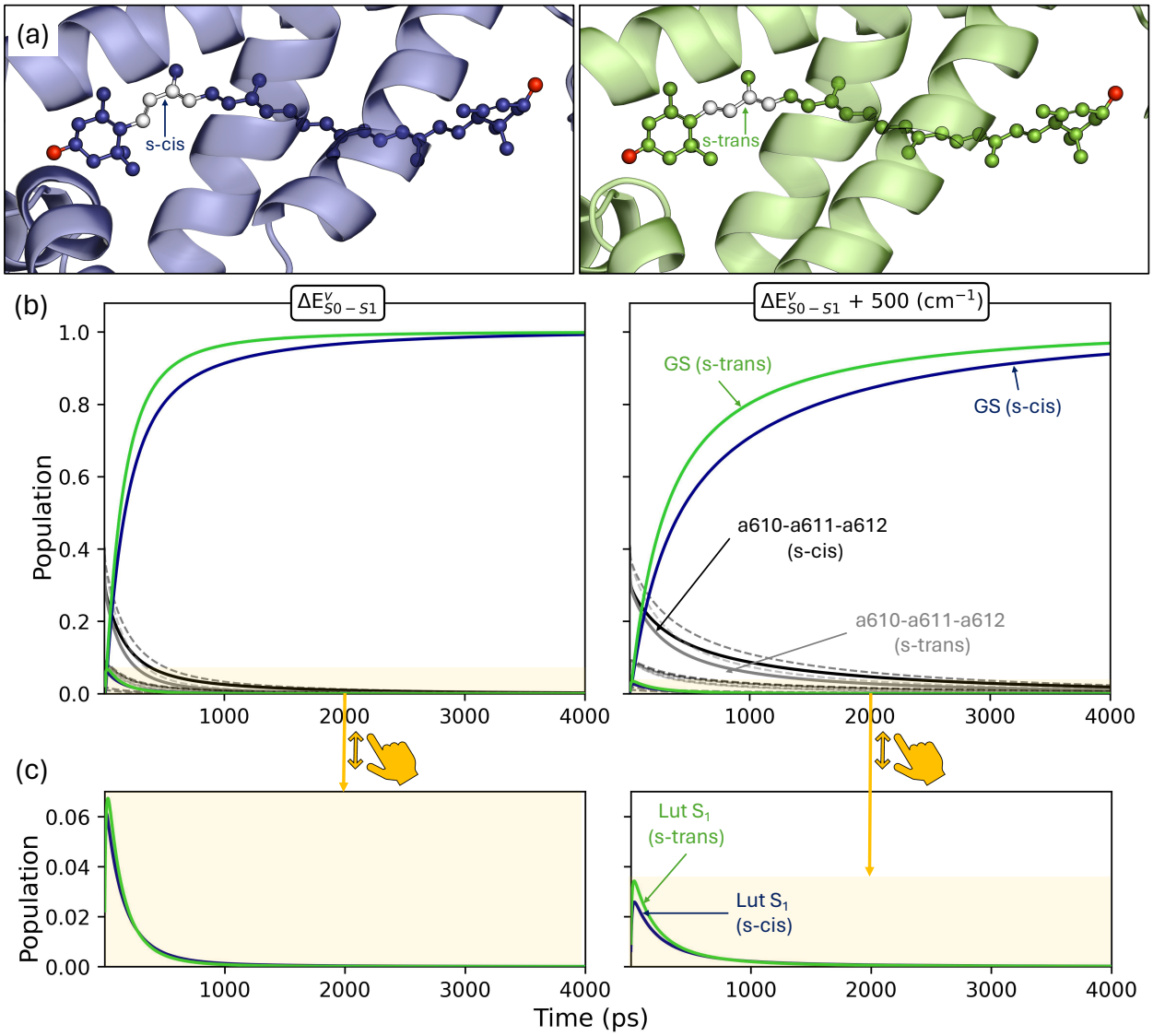

Figure 6: Effect of the S_1 vertical excitation energy as well as the Lut conformation on the population dynamics of CP29 complex. (a) Representation of s-cis and s-trans conformations of Lut in CP29 (b) All pigment EET average populations for CP29 structures featuring s-cis (blue) and s-trans (green) Lut conformations. The populations of the ground-state are depicted in blue for s-cis and green for s-trans. Populations of the Chl exciton a610-a611-a612 are shown for s-cis (black continuous line) and s-trans (gray continuous line), while the populations of the other Chl excitons are shown as dashed lines using the same color notation. (c) Zoomed-in region of Lut S_1 populations, s-cis (blue) and s-trans (green).

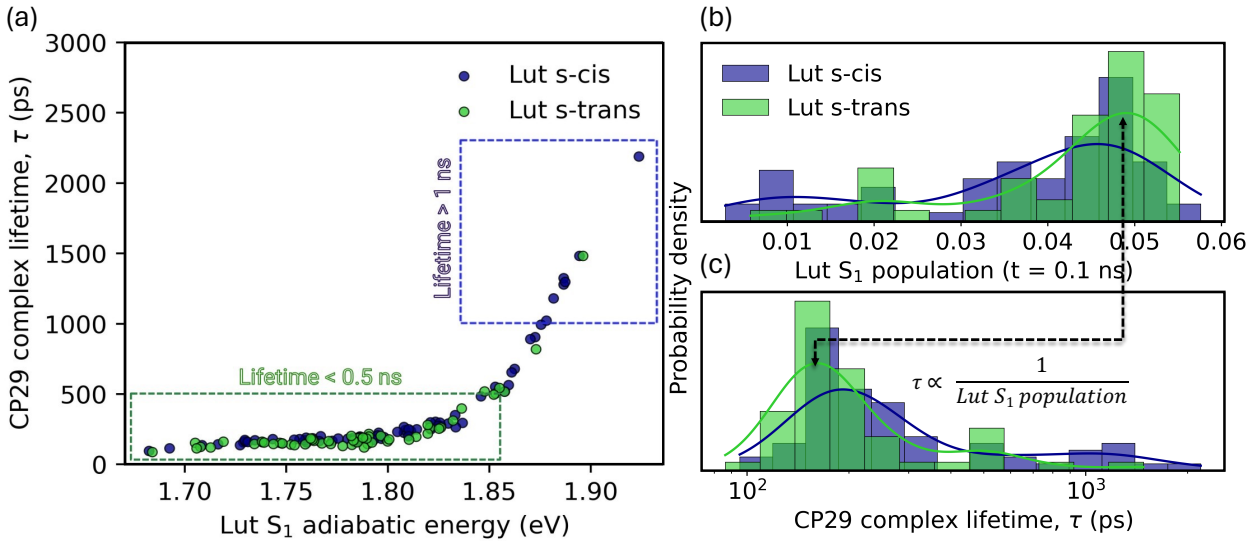

Figure 7: The effect of Lut conformation on the EET mechanism. (a) The variation of the excited-state lifetime with respect to the S_1 adiabatic energies for CP29 geometries with s-cis and s-trans conformers. (right panel) The probability distribution of (b) Lut S1 population at 0.1 ns and (c) the excited-state lifetime of the s-cis and s-trans conformers.

understand the factors influencing the S_1 energy. Second, a comprehensive understanding of Lut distortion and the conformation of the binding pocket requires quantitative sampling of accurate structures. Our current approach relies on semiempirical QM/MM refinement of structures derived from fully classical enhanced sampling simulations, which may over- or under-represent certain configurations, potentially biasing the results.

4 Conclusions

We have developed a computational protocol to calculate excitation-energy transfer quenching by carotenoids in light-harvesting complexes. Specifically, our quenching model is based on EET from excited chlorophylls to the lowest dark singlet state (S_1) of Lut. This was done using a kinetic model that includes the entire Chl aggregate along with the Lut S_1 state.

One of the main challenges in modeling the EET pathway for quenching is the uncertainty surrounding both the lineshape and the adiabatic energy of the Lut S_1 state. While experimental data fitting is typically used to address these uncertainties, in this work we

compute the spectral density — and, by extension, the lineshape — of the dark S_1 state of Lut from calculations. This represents a significant difference from existing methodologies as well as a novelty of this work.

We applied our strategy to CP29, one of the minor light-harvesting complex of plants, which exhibits conformationally driven variations in the excited-state lifetime.[9] Our kinetic model revealed an extremely sensitive EET rate that strongly depends on the Lut S_1 adiabatic energy, with the excited-state lifetime varying from the picosecond regime to nanoseconds. This is consistent with the existing literature reporting on the role of Lut S_1 in the regulation of EET quenching. Furthermore, we investigated whether the Lut conformation influences the excited-state lifetime and, consequently, the extent of quenching. Though we observed a slightly larger proportion of Lut s-trans geometries in the quenched state, a definitive evidence for the tuning of the complex from the light-harvesting to the quencher state through a conformational change of Lut would require a more quantitative sampling of accurate structures.

The computational methodology developed in this work is also applicable to studying EET processes in other light-harvesting complexes and offers a promising approach to addressing the unresolved question of the molecular mechanisms underlying nonphotochemical quenching.

Acknowledgement

L.C. and B.M. acknowledge financial support from Italian MUR through the PRIN 2022 grant 2022N8PBLM (PhotoControl). C.J and B.M. acknowledge funding by the MUR - FARE Ricerca through the project "Quantum-LIP". The authors acknowledge Dr. Davide Accomasso for providing the structures of CP29 sampled from ground-state QM/MM thermal equilibrations, and Piermarco Saraceno for his assistance with the Redfield-Förster calculations.

Supporting Information Available

Details of the kinetic model; $S_1 \rightarrow S_n$ excited-state absorption spectra (ESA) of Lut in CP29.

References

(1) Croce, R.; van Amerongen, H. Natural Strategies for Photosynthetic Light Harvesting. *Nat. Chem. Biology* **2014**, *10*, 492–501.

(2) Pascal, A. A.; Liu, Z.; Broess, K.; van Oort, B.; van Amerongen, H.; Wang, C.; Horton, P.; Robert, B.; Chang, W.; Ruban, A. Molecular Basis of Photoprotection and Control of Photosynthetic Light-Harvesting. *Nature* **2005**, *436*, 134–137.

(3) Pinnola, A.; Bassi, R. Molecular Mechanisms Involved in Plant Photoprotection. *Biochem. Soc. Trans.* **2018**, *46*, 467–482.

(4) Li, Z.; Wakao, S.; Fischer, B. B.; Niyogi, K. K. Sensing and Responding to Excess Light. *Annu. Rev. Plant Biol.* **2009**, *60*, 239–260.

(5) Niyogi, K. K.; Truong, T. B. Evolution of Flexible Non-Photochemical Quenching Mechanisms that Regulate Light Harvesting in Oxygenic Photosynthesis. *Curr. Opin. Plant Biol.* **2013**, *16*, 307–314.

(6) Ruban, A. V.; Johnson, M. P.; Duffy, C. D. The Photoprotective Molecular Switch in the Photosystem II Antenna. *Biochim. Biophys. Acta (BBA) - Bioenergetics* **2012**, *1817*, 167–181.

(7) Ruban, A. V. Light Harvesting Control in Plants. *FEBS Lett.* **2018**, *592*, 3030–3039.

(8) Bennett, D. I. G.; Amarnath, K.; Park, S.; Steen, C. J.; Morris, J. M.; Fleming, G. R. Models and Mechanisms of the Rapidly Reversible Regulation of Photosynthetic Light Harvesting. *Open Biology* **2019**, *9*.

(9) Mascoli, V.; Liguori, N.; Xu, P.; Roy, L. M.; van Stokkum, I. H.; Croce, R. Capturing the Quenching Mechanism of Light-Harvesting Complexes of Plants by Zooming in on the Ensemble. *Chem* **2019**, *5*, 2900–2912.

(10) Krüger, T. P.; Ilioaia, C.; Johnson, M. P.; Ruban, A. V.; Papagiannakis, E.; Horton, P.; van Grondelle, R. Controlled Disorder in Plant Light-Harvesting Complex II Explains Its Photoprotective Role. *Biophysical J.* **2012**, *102*, 2669–2676.

(11) Liguori, N.; Xu, P.; van Stokkum, I. H.; van Oort, B.; Lu, Y.; Karcher, D.; Bock, R.; Croce, R. Different Carotenoid Conformations have Distinct Functions in Light-Harvesting Regulation in Plants. *Nat. Commun.* **2017**, *8*.

(12) Son, M.; Pinnola, A.; Gordon, S. C.; Bassi, R.; Schlau-Cohen, G. S. Observation of Dissipative Chlorophyll-to-Carotenoid Energy Transfer in Light-Harvesting Complex II in Membrane Nanodiscs. *Nat. Commun.* **2020**, *11*.

(13) Park, S.; Fischer, A. L.; Li, Z.; Bassi, R.; Niyogi, K. K.; Fleming, G. R. Snapshot Transient Absorption Spectroscopy of Carotenoid Radical Cations in High-Light-Acclimating Thylakoid Membranes. *J. Phys. Chem. Lett.* **2017**, *8*, 5548–5554.

(14) Dall'Osto, L.; Cazzaniga, S.; Bressan, M.; Paleček, D.; Židek, K.; Niyogi, K. K.; Fleming, G. R.; Zigmantas, D.; Bassi, R. Two Mechanisms for Dissipation of Excess Light in Monomeric and Trimeric Light-Harvesting Complexes. *Nat. Plants* **2017**, *3*.

(15) Guardini, Z.; Bressan, M.; Caferri, R.; Bassi, R.; Dall'Osto, L. Identification of a Pigment Cluster Catalysing Fast Photoprotective Quenching Response in CP29. *Nat. Plants* **2020**, *6*, 303–313.

(16) Schlau-Cohen, G. S.; Yang, H.-Y.; Krüger, T. P. J.; Xu, P.; Gwizdala, M.; van Grondelle, R.; Croce, R.; Moerner, W. E. Single-Molecule Identification of Quenched and Unquenched States of LHCII. *J. Phys. Chem. Lett.* **2015**, *6*, 860–867.

(17) Ahn, T. K.; Avenson, T. J.; Ballottari, M.; Cheng, Y.-C.; Niyogi, K. K.; Bassi, R.; Fleming, G. R. Architecture of a Charge-Transfer State Regulating Light Harvesting in a Plant Antenna Protein. *Science* **2008**, *320*, 794–797.

(18) Bode, S.; Quentmeier, C. C.; Liao, P.-N.; Hafi, N.; Barros, T.; Wilk, L.; Bittner, F.; Walla, P. J. On the Regulation of Photosynthesis by Excitonic Interactions between Carotenoids and Chlorophylls. *Proc. Natl. Acad. Sci.* **2009**, *106*, 12311–12316.

(19) Chmeliov, J.; Bricker, W. P.; Lo, C.; Jouin, E.; Valkunas, L.; Ruban, A. V.; Duffy, C. D. P. An 'All Pigment' Model of Excitation Quenching in LHCII. *Phys. Chem. Chem. Phys.* **2015**, *17*, 15857–15867.

(20) Fox, K. F.; Balevičius, V.; Chmeliov, J.; Valkunas, L.; Ruban, A. V.; Duffy, C. D. P. The Carotenoid Pathway: What is Important for Excitation Quenching in Plant Antenna Complexes? *Phys. Chem. Chem. Phys.* **2017**, *19*, 22957–22968.

(21) Daskalakis, V.; Maity, S.; Hart, C. L.; Stergiannakos, T.; Duffy, C. D. P.; Kleinekathöfer, U. Structural Basis for Allosteric Regulation in the Major Antenna Trimer of Photosystem II. *J. Phys. Chem. B* **2019**, *123*, 9609–9615.

(22) Fox, K. F.; Ünlü, C.; Balevičius, V.; Ramdour, B. N.; Kern, C.; Pan, X.; Li, M.; van Amerongen, H.; Duffy, C. D. A Possible Molecular Basis for Photoprotection in the Minor Antenna Proteins of Plants. *Biochim. Biophys. Acta (BBA) - Bioenergetics* **2018**, *1859*, 471–481.

(23) Lapillo, M.; Cignoni, E.; Cupellini, L.; Mennucci, B. The Energy Transfer Model of Nonphotochemical Quenching: Lessons from the Minor CP29 Antenna Complex of Plants. *Biochim. Biophys. Acta (BBA) - Bioenerg.* **2020**, *1861*, 148282.

(24) Cignoni, E.; Lapillo, M.; Cupellini, L.; Acosta-Gutiérrez, S.; Gervasio, F. L.; Mennucci, B. A Different Perspective for Nonphotochemical Quenching in Plant Antenna Complexes. *Nat. Commun.* **2021**, *12*, 1–9.

(25) Sardar, S.; Caferri, R.; Camargo, F. V.; Pamos Serrano, J.; Ghezzi, A.; Capaldi, S.; Dall'Osto, L.; Bassi, R.; D'Andrea, C.; Cerullo, G. Molecular Mechanisms of Light Harvesting in the Minor Antenna CP29 in Near-Native Membrane Lipidic Environment. *J. Chem. Phys.* **2022**, *156*.

(26) Sardar, S.; Caferri, R.; Camargo, F. V.; Capaldi, S.; Ghezzi, A.; Dall'Osto, L.; D'Andrea, C.; Cerullo, G.; Bassi, R. Site-Directed Mutagenesis of the Chlorophyll-Binding Sites Modulates Excited-State Lifetime and Chlorophyll–Xanthophyll Energy Transfer in the Monomeric Light-Harvesting Complex CP29. *J. Phys. Chem. Lett.* **2024**, *15*, 3149–3158.

(27) Accomasso, D.; Londi, G.; Cupellini, L.; Mennucci, B. The Nature of Carotenoid S* State and its Role in the Nonphotochemical Quenching of Plants. *Nat. Commun.* **2024**, *15*, 847.

(28) Saraceno, P.; Sláma, V.; Cupellini, L. First-Principles Simulation of Excitation Energy Transfer and Transient Absorption Spectroscopy in the CP29 Light-Harvesting Complex. *J. Chem. Phys* **2023**, *159*.

(29) Lee, M. K.; Huo, P.; Coker, D. F. Semiclassical Path Integral Dynamics: Photosynthetic Energy Transfer with Realistic Environment Interactions. *Annu. Rev. Phys. Chem.* **2016**, *67*, 639–668.

(30) Cupellini, L.; Corbella, M.; Mennucci, B.; Curutchet, C. Electronic Energy Transfer in Biomacromolecules. *Wiley Interdiscip. Rev. Comput. Mol. Sci.* **2019**, *9*, e1392.

(31) Wei, X.; Su, X.; Cao, P.; Liu, X.; Chang, W.; Li, M.; Zhang, X.; Liu, Z. Structure of Spinach Photosystem II–LHCII Supercomplex at 3.2 Å Resolution. *Nature* **2016**, *534*, 69–74.

(32) Maier, J. A.; Martinez, C.; Kasavajhala, K.; Wickstrom, L.; Hauser, K. E.; Simmer-

ling, C. ff14SB: Improving the Accuracy of Protein Side Chain and Backbone Parameters from ff99SB. *J. Chem. Theory Comput.* **2015**, *11*, 3696–3713.

(33) Dickson, C. J.; Madej, B. D.; Skjevik, A. A.; Betz, R. M.; Teigen, K.; Gould, I. R.; Walker, R. C. Lipid14: The Amber Lipid Force Field. *J. Chem. Theory Comput.* **2014**, *10*, 865–879.

(34) Mark, P.; Nilsson, L. Structure and Dynamics of the TIP3P, SPC, and SPC/E Water Models at 298 K. *J. Phys. Chem. A* **2001**, *105*, 9954–9960.

(35) Zhang, L.; Silva, D.-A.; Yan, Y.; Huang, X. Force Field Development for Cofactors in the Photosystem II. *J. Comput. Chem.* **2012**, *33*, 1969–1980.

(36) Prandi, I. G.; Viani, L.; Andreussi, O.; Mennucci, B. Combining Classical Molecular Dynamics and Quantum Mechanical Methods for the Description of Electronic Excitations: The Case of Carotenoids. *J. Comput. Chem.* **2016**, *37*, 981–991.

(37) Frisch, M. J. et al. Gaussian 16 Revision A.03. 2016; Gaussian Inc. Wallingford CT.

(38) Accomasso, D.; Arslancan, S.; Cupellini, L.; Granucci, G.; Mennucci, B. Ultrafast Excited-State Dynamics of Carotenoids and the Role of the S_X State. *J. Phys. Chem. Lett.* **2022**, *13*, 6762–6769.

(39) Pedraza-González, L.; Cignoni, E.; D'Ascenzi, J.; Cupellini, L.; Mennucci, B. How the pH Controls Photoprotection in the Light-Harvesting Complex of Mosses. *J. Am. Chem. Soc.* **2023**, *145*, 7482–7494.

(40) Arcidiacono, A.; Accomasso, D.; Cupellini, L.; Mennucci, B. How Orange Carotenoid Protein Controls the Excited State Dynamics of Canthaxanthin. *Chem. Sci.* **2023**, *14*, 11158–11169.

(41) Pedraza-González, L.; Accomasso, D.; Cupellini, L.; Granucci, G.; Mennucci, B. Ultrafast Excited-State Dynamics of Luteins in the Major Light-Harvesting Complex LHCII. *Photochem. Photobiol. Sci* **2024**, *23*, 303–314.

(42) Granucci, G.; Toniolo, A. Molecular Gradients for Semiempirical CI Wavefunctions with Floating Occupation Molecular Orbitals. *Chem. Phys. Lett.* **2000**, *325*, 79–85.

(43) Stewart, J. J. P. MOPAC2002; Fujitsu Limited: Tokyo, Japan. 2002.

(44) Ponder, J. W. TINKER — Software Tools for Molecular Design, Version 6.3, Copyright (c). February 2014.

(45) Llansola-Portoles, M. J.; Pascal, A. A.; Robert, B. Electronic and Vibrational Properties of Carotenoids: From in vitro to in vivo. *J. Royal Soc. Interface* **2017**, *14*, 20170504.

(46) Das, S. K.; Frank, H. A. Pigment Compositions, Spectral Properties, and Energy Transfer Efficiencies between the Xanthophylls and Chlorophylls in the Major and Minor Pigment-Protein Complexes of Photosystem II. *Biochem.* **2002**, *41*, 13087–13095.

(47) Saraceno, P.; Cupellini, L. pyQME: a Package for Open Quantum System Dynamics and Spectroscopies Simulations in the Exciton Framework. 2024; `https://github.com/Molecolab-Pisa/pyQME`.

(48) Avila Ferrer, F. J.; Santoro, F. Comparison of Vertical and Adiabatic Harmonic Approaches for the Calculation of the Vibrational Structure of Electronic Spectra. *Phys. Chem. Chem. Phys.* **2012**, *14*, 13549.

(49) Chen, W.-C.; Cheng, Y.-C. Elucidating the Magnitude of Internal Reorganization Energy of Molecular Excited States from the Perspective of Transition Density. *J. Phys. Chem. A* **2020**, *124*, 7644–7657.

(50) Blumberger, J. Recent Advances in the Theory and Molecular Simulation of Biological Electron Transfer Reactions. *Chem. Rev.* **2015**, *115*, 11191–11238.

(51) Scholes, G. D.; Jordanides, X. J.; Fleming, G. R. Adapting the Förster Theory of Energy Transfer for Modeling Dynamics in Aggregated Molecular Assemblies. *J. Phys. Chem. B* **2001**, *105*, 1640–1651.

(52) Saraceno, P.; Sardar, S.; Caferri, R.; Camargo, F. V. A.; Dall'Osto, L.; D'Andrea, C.; Bassi, R.; Cupellini, L.; Cerullo, G.; Mennucci, B. Probing the Effect of Mutations on Light Harvesting in CP29 by Transient Absorption and First-Principles Simulations. *J. Phys. Chem. Lett.* **2024**, *15*, 6398–6408, PMID: 38861672.

(53) Polívka, T.; Sundström, V. Ultrafast Dynamics of Carotenoid Excited States−From Solution to Natural and Artificial Systems. *Chem. Rev.* **2004**, *104*, 2021–2072.